**RHEOLOGICAL AND MICROSTRUCTURAL INVESTIGATION OF ILMENITE-OLIVINE AGGREGATES DEFORMED IN SHEAR: IMPLICATIONS FOR LUNAR MANTLE CUMULATE OVERTURN**. N.L. Grambling[1], L. Tokle[2,3], N. Dygert[1], G. Hirth[3], E. Chin[4], Y. Liang[3], C. Meyers[3], [1]Earth and Planetary Sciences, University of Tennessee, Knoxville, TN 37916, USA (ngrambli@vols.utk.edu); [2]ETH Zürich, Earth Sciences, Zürich, Switzerland; [3]Earth, Environmental, and Planetary Sciences, Brown University, Providence, RI 02912, USA; [4]Scripps Institution of Oceanography, San Diego, CA 92037, USA

We investigate the rheological and microstructural properties of aggregates of ilmenite and olivine deformed in shear in a Griggs apparatus. The experiments constrain the effective viscosity of an ilmenite-bearing lunar mantle as a function of ilmenite content and shear strain. Ilmenite exhibits viscous anisotropy, deforming by basal slip in shear, and is very weak relative to dry olivine. Small amounts of ilmenite weaken an ilmenite-olivine aggregate, suggesting lunar cumulate mantle overturn would occur in long wavelength instabilities.

**Background:** During or shortly after solidification of a lunar magma ocean (LMO), the lunar mantle is proposed to have undergone cumulate mantle overturn [1]. The overturn model posits that an initially shallow, thin, and dense layer of ilmenite (ilm)-rich cumulates beneath an anorthositic flotation crust sank as viscous solids into underlying, earlier crystallized olivine cumulates, forming a thicker layer of ilmenite-bearing cumulates (IBC). The IBC then sank deeper into the lunar mantle, forming the sources of high-Ti basalts [2]. The wavelength ($\lambda$) of overturning instabilities depends on the thickness of the IBC layer ($h$) and the viscosity contrast between the IBC and underlying cumulates:

$$\lambda = 2.9h\left(\frac{\mu_{mafic}}{\mu_{IBC}}\right)^{\frac{1}{3}} \quad (1)$$

[3]. Thus, knowledge of the viscosity contrast between the IBC and underlying mafic cumulates is critical for modeling early lunar evolution.

**Starting materials:** Synthetic ilmenite ($FeTiO_3$) utilized in this study was purchased from Sigma Aldrich, then synthesized in a mixture with MgO reagent oxide powder in Deltech gas mixing furnace at Brown University to form ilmenite40 (ilm40; $Mg_{0.6}Fe_{0.4}TiO3$) in the ilmenite-geikielite system. This composition is in equilibrium with olivine representative of early LMO cumulates, which has an Mg# of ~90 [4, 5]. Natural Scan Carlos olivine (ol, Mg# 90) was utilized to form ilm40-ol mixtures. Grain size ranges of 10 to 20 µm were used for both ilm40 and ol and were separated by Stokes' settling and sieving. Constituent phase weights were calculated from target volume ratios and mechanically mixed prior to packing powders in Ni experimental jackets.

**Experiments:** Experiments were conducted using a Griggs deformation apparatus at Brown University. We utilized molten salt assemblies and alumina shear pistons at 1 GPa confining pressure and 1100°C. Experiments were deformed at an axial displacement rate of $9.2\times10^{-4}$ mm/sec corresponding to a shear strain rate of ~$1\times10^{-6}$. Experiments are summarized in Table 1.

**Table 1.** Experiments, axial equivalent differential stress ($\sigma_D$) and total strain ($\varepsilon$) upon quench.

| Name | Ilm:Ol | $\sigma_D$ (MPa) | ɣ |
|---|---|---|---|
| LMO001 | 100:0 | 101 | 1.23 |
| LMO002 | 10:90 | 233 | 0.54 |
| LMO003 | 10:90 | 205 | 1.38 |
| LMO004 | 50:50 | 141 | 0.85 |
| LMO005 | 25:75 | 311 | 0.82 |

In addition to a pure ilm40 experiment, four ratios of ilm40:ol were tested thus far: 50:50 ilm40:ol; 25:75 ilm40:ol and 10:90 ilm40:ol. The 10:90 proportion was tested twice to produce high and low total strain samples. Recovered mechanical data were used to calculate axial equivalent differential stresses and strains (Fig. 1) using a modified version of the RIG program [6]. The experiments exhibit significant variability in shear stress according to their ilm40 contents. The correlation of aggregate strength with ilm40 proportion suggests the rheology of the aggregate is strongly influenced by the weaker material, ilm40. We observe that in some experiments, strength decreases from an initial peak as strain progresses. The 25:75 ilm40:Ol experiment is anomalously stronger than the other experiments (even the 10:90 experiments), and will be repeated in future work.

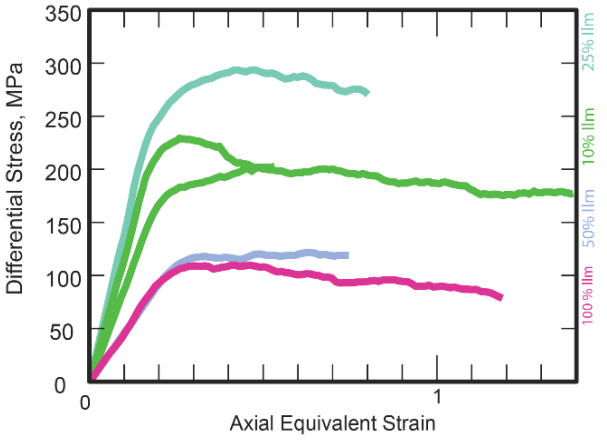


*Figure 1. Axial Equivalent Strain vs. Differential Stresses. Percent ilm40 in each experiment is indicated by color and labeled right of the plot along the y-axis.*

**Fabric and Microstructural Analysis:** Backscatter electron micrographs of sectioned, polished run products were collected by Scanning Electron Microscope at the

University of Tennessee. Representative examples of the low and high strain 10:90 experiments are shown in Fig. 2. Comparison of ilm40 grains suggests morphological evolution as deformation progresses. The ilm40 grains flatten and become elongated within the shear plane.

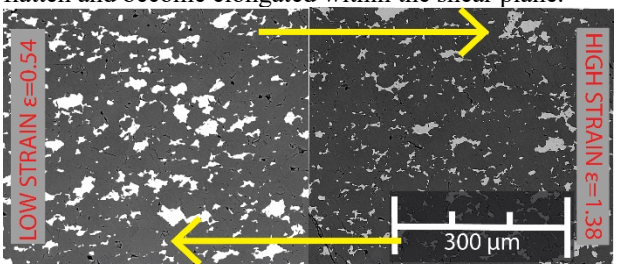


*Figure 2. Photomicrographs of the 10% ilm40: 90% Ol samples. The lower total strain sample is on the left and the higher total strain sample is on the right. Bright phase is ilm40, dark phase is ol and shear sense is shown by yellow arrows.*

Crystallographic orientations of minerals in the experiments were determined by electron backscatter diffraction (EBSD) at Scripps Institution of Oceanography. Lower hemisphere equal area pole figures for olivine (a,b and c axes) and ilmenite (c-axis only) are shown in Fig. 3 for the low and high strain 10:90 experiments (top and bottom, respectively). Comparison of the low and high strain samples suggests crystallographic preferred orientations (CPOs) become better defined as strain progresses, as seen from the contouring patterns (especially olivine a and b axes, and ilmenite c axes). The orientations of the olivine grains are consistent with a "B-type" fabric [e.g., 7, 8], traditionally interpreted to represent deformation under high stress, "wet" conditions.

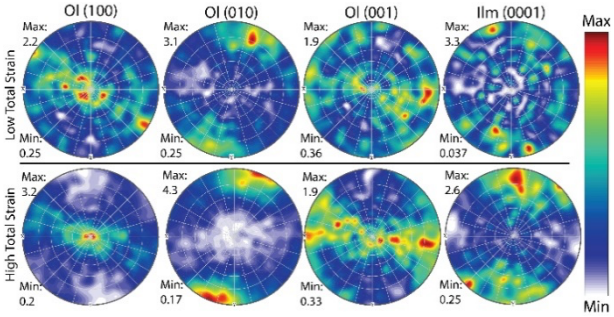


*Figure 3. Representative pole figures for low (top) and high (bottom) total strain 10:90 experiments. Cooler and hotter colors represent low- and high-density axis orientations.*

**Comparison to pure phase deformation experiments and flow laws:** Axial equivalent differential stresses and strain rates of our experiments are compared to pure phase ilmenite and ilm40 experiments deformed in axial compression [11,12] in Fig. 4. Flow laws for wet (1000 H/$10^6$Si; 62.5ppm $H_2O$) and dry olivine [9,10], ilmenite and ilm40 [11,12] are also shown. The shear experiments plot between the ilmenite and ilm40 data (except for the 25:75 experiment). Surprisingly, the 100% ilm40 shear experiment (magenta circle) plots with the ilmenite axial compression data (+ symbols). The 10:90 shear experiments plot with the ilm40 axial compression experiments (triangles) and the 50:50 experiment plots between the pure phase axial compression experiments. The comparison suggests that ilm40 is viscously anisotropic. The ilmenite pole figures show c axis orientations perpendicular to the shear plane (Fig. 3). We infer that ilm40 deformation in the shear experiments dominantly occurred by basal slip, consistent with the layered structure of ilmenite-group minerals.

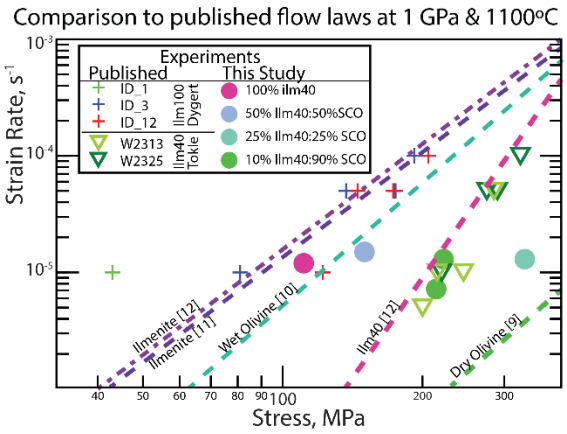


*Figure 4. Comparison of our experimental results (filled circles, same colors as Fig. 1) to pure phase ilmenite (+ symbols [11]) and ilm40 experiments (triangles, [12]) deformed in axial compression. All experiments shown were conducted at 1100°C and 1GPa confining pressure. Dashed lines show predictions of published flow laws (dry olivine (green), wet olivine (blue) [H&K], ilmenite100 [Dygert], ilmenite40 [Tokle].*

**Inferences:** Our experimental results demonstrate that the presence of ilmenite in an olivine-rich cumulate mantle could greatly reduce its effective viscosity, facilitating low spherical harmonic degree cumulate mantle overturn [13].

**References:** [1] Hess & Parmentier, 1995. EPSL 134, 501-514. [2] Ringwood & Kesson, 1976. LPSC 7, 1697-1722. [3] Whitehead, 1988. Ann. Rev. of Fluid Mech., 20(1), 61–87. [4] Andersen & Lindsley, 1979. LPSC 10, 493-507. [5] Thacker et al., 2009. GCA 73, 820-836. [6] Pec, 2010. RIG: a MATLAB™ program for evaluation of mechanical data from experimental apparatuses. [7] Bernard et al., 2019 G3, 20, 34693494. [8] Karato et al., 2008. Ann. Rev. of Earth & Planet. Sci., 36, 59-95. [9] Hirth & Kohlstedt, 1996. EPSL, 144, 93-108. [10] Hirth & Kohlstedt, 2003; Geophys. Monograph 138, 83-105. [11] Dygert, Hirth, Liang, 2016. GRL 43. [12] Tokle et al., 2021. JGR-Planets 126. [13] Li et al., 2019. JGR-Planets 124, 1357-13.